

A Simple Fluorescence Sensor Based on Merocyanine 540-MnO₂ System to Detect Hypochlorite

Ayşe Merve Şenol^{1*} 

¹Program of Medical Laboratory Techniques, Department of Medical Services and Techniques, University of Health Sciences, Istanbul 34668, Türkiye

*aysemerve.senol@sbu.edu.tr

* Orcid No: 0000-0003-3355-8222

Received: 1 November 2023

Accepted: 7 February 2024

DOI: 10.18466/cbayarfbe.1384266

Abstract

Merocyanine 540 (MC540)- Manganese oxide (MnO₂) system-based fluorescence sensor is reported as an anion sensor in aqueous solution. MnO₂ was synthesized in the presence of Potassium permanganate (KMnO₄) and Cetyltrimethylammonium bromide (CTAB) using 3-(N-morpholino) propane sulfonic acid (MOPS) buffer. The formation of MnO₂ was first confirmed by a color change and characterized using X-ray diffraction (XRD), Fourier transform infrared spectroscopy (FTIR), and Ultraviolet-Visible (UV-Vis) absorption spectroscopy techniques. Next, the interaction of MC540 with MnO₂ in aqueous solution was investigated at various conditions by UV-Vis. absorption and fluorescence spectroscopy. The sensing ability of the MC540-MnO₂ was tested to detect hypochlorite (ClO⁻) ion as a “Turn-off” fluorescent sensor. The MC540-MnO₂ revealed to be high selectivity and sensitivity to detect hypochlorite (ClO⁻) ion without being affected by the other thirteen anions. The detection limits for ClO⁻ were evaluated in two different concentration ranges and calculated to be 0.14 µM at 0.33-4.46 µM and 0.38 µM at 5.06-14.30 µM, respectively.

Keywords: Anionic dye, Anions, Fluorescence quantum yield, Fluorescence quenching, Fluorescence sensor, Hypochlorite, MnO₂

1. Introduction

Organic fluorescent dyes attract the attention of researchers because they have many applications, including organic light-emitting diodes, bioimaging, fluorescence-image, and fluorescence sensors [1-4]. Merocyanine 540 (MC540), a water-soluble organic fluorescent anionic dye, consists of a benzoxazole skeleton and a hexahydropyrimidine-3,5-dione-2-thion ring linked by a conjugated triene (Fig. 1). As with many other fluorescent organic dyes, MC540 has attracted a lot of interest due to its cheap and easy design. The MC540's optical properties could change as a result of interactions with themselves or various semiconductors [5], graphene-based material [6], clays, nanostructures [7], and polyelectrolytes [8]. These changes are determined by absorption and fluorescence spectroscopy [4]. Thus, such newly designed systems can be used in various applications such as solar cells [5], photodynamic therapy[9], chemotherapy [7], and fluorescence sensors [6, 10].

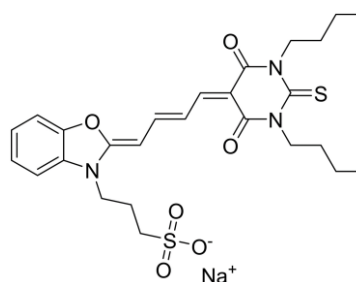


Figure 1. Molecular structure of MC540

Manganese oxide (MnO₂), a prevalent transition metal oxide is absorbed in a wide wavelength range, nontoxic, and readily modified [11]. Moreover, it is one of the most promising conductive materials in various industries such as batteries, water treatment plants, and catalysis due to its low-cost, high-energy density, and ecological compatibility [12]. In addition, when MnO₂ is added to fluorescent materials, it can be subjected to molecular aggregation owing to various molecular interactions (electrostatic, hydrogen bonding, and hydrophobic interactions, etc.) which change the spectral behavior of

the dye [13]. Thus, various new fluorescence probe (dye- MnO_2) systems can be prepared. In recent years, sensor systems based on molecular aggregation of various fluorescent materials in the presence of MnO_2 have attracted attention. For example; fluorescent perylene- MnO_2 to detect acetylcholinesterase (AChE) [11], fluorescent carbon dots- MnO_2 platform to detect glutathione (GSH) [14, 15], fluorescent polydopamine nanoparticles- MnO_2 to detect alkaline phosphatase [16], fluorescent gold clusters- MnO_2 to detect H_2O_2 [17], and fluorescent fluorescein dye- MnO_2 to detect H_2O_2 [18]. However, no fluorescent sensor studies with cyanine-derived dye in the presence of MnO_2 have been found in the literature.

Hypochlorite (ClO^-) is an important reactive oxygen species that plays a significant role in the biological process of living organisms. ClO^- , which can be taken directly into our body without being aware of it, is widely used for disinfection and sterilization in swimming pools, tap water, and almost all surfaces. Its deficiency or abundance causes various diseases. Excess ClO^- can induce kidney, neurological function, cardiovascular system, and cancer, whereas inadequate chlorate can cause many serious diseases as it fails to kill pathogens. Therefore, ClO^- is very important to detect as quantitative by a practical method [19]. Until now, it has been determined in many methods, including ICP-AES/MS, HPLC, electrochemical, colorimetric, and fluorescence sensors, etc. Among them, the fluorescence sensor technique has drawn attention owing to its high speed, stability, selectivity, and accuracy, as well as economical and practical. In recent years, the design of new fluorescent sensors that can detect various anions and cations, especially in aqueous media, has been of great attention. Therefore, these types of sensors still need to be developed [14].

In the present study, a novel “Turn-off” fluorescence sensor is reported to detect precisely and selectively ClO^- ions based on the interaction of MC540 with MnO_2 in an aqueous solution. Firstly, MnO_2 was synthesized in the presence of KMnO_4 and CTAB using MOPS buffer. The formation of MnO_2 was first observed by a color change and analyzed by XRD, FTIR, and absorption spectroscopy. Secondly, the interaction of MC540 with

MnO_2 in aqueous solution was investigated using UV-Vis. absorption and fluorescence spectroscopy at various conditions, and the MC540- MnO_2 system as a fluorescent probe was determined. Thirdly, the sensing ability of the MC540- MnO_2 was tested to detect anions as a “Turn-off” fluorescent sensor in the presence of fourteen anions, and LOD values in two different concentration ranges for ClO^- were calculated. Also, interference tests for ClO^- were carried out.

2. Materials and Methods

2.1. Materials

Potassium permanganate (KMnO_4), Cetyltrimethylammonium bromide (CTAB), MOPS (3-(N-morpholino) propane sulfonic acid) used in MnO_2 synthesis; all anion sodium salts (NaF , NaBr , NaI , NaCl , Na_2SO_4 , $\text{Na}_2\text{CO}_3 \cdot \text{H}_2\text{O}$, Na_3PO_4 , NaNO_3 , Na_2S , NaCN , NaSCN , $\text{Na}_2\text{C}_2\text{O}_4$, CH_3COONa , and NaClO) used in fluorescence sensor experiments; MC 540 and Rhodamine 101(Rh 101) dyes were purchased from Merck KGaA, Germany. These chemicals were used as received.

2.2. Synthesis of MnO_2

MnO_2 was synthesized in the presence of KMnO_4 and CTAB using MOPS buffer instead of MES(2-(N-morpholino) ethane sulfonic acid) buffer by partially modifying a previous method in the literature [14]. Firstly, KMnO_4 (0.5 g) was dissolved in 0.45 L of distilled water for 30 min. The color of the solution is dark purple. Secondly, CTAB (1.5 g) was added to the solution and mixed for 10 minutes, resulting in a light purple color. Thirdly, MOPS buffer (50 ml at pH 6.5, 0.1 M) was added dropwise over half an hour, and the color of the solution changed from light purple to light brown as MOPS was added. The resulting mixture was stirred for 13 hours and its color was dark brown-black (Fig. 2). The stirring speed is 700 rpm. The obtained MnO_2 solution was centrifuged for 15 min at 9500 rpm. The MnO_2 NPs were collected after centrifugation by washing three times with distilled water and ethanol, respectively.



Figure 2. Synthesis of MnO_2

2.3. Instruments

FT-IR spectra were recorded by a Bruker Alpha ATR spectrometer, in the wavenumbers ranging from 400 cm^{-1}

to 4000 cm^{-1} (Bruker Corporation, U.S.A.). XRD analysis was collected by a PANalytical's X-ray diffractometers in the 2θ range of 10° - 90° (Panalytical, Netherlands). Fluorescence spectra were taken on

Agilent Technologies Cary Eclipse Fluorescence Spectrophotometer at an excitation wavelength (λ_{ex}) of 500 nm (Agilent Technologies, U.S.A.). Absorption spectra were recorded on Shimadzu UV-1800 spectrophotometer (Shimadzu, Japan).

2.4. Calculations

The relative fluorescence quantum yields (Φ_f) of the MC540-MnO₂ systems in an aqueous solution were determined by the Parker-Rees method using Rh 101 ($\Phi_f = 1.0$ in methanol) as reference dye [6].

Also, the ClO⁻ sensitivity of the MC540-MnO₂ system is tested by using the Stern-Volmer equation (Eq. 1). The limit of detection (LOD) for ClO⁻ was calculated using the slope and standard deviation of this plot.

$$\frac{F_0}{F} = 1 + K_{SV}[Q] \quad (1)$$

Herein, K_{SV} is the Stern-Volmer constant; $[Q]$ is a quencher ([ClO⁻] in this study); F_0 and F are the fluorescence intensity (λ_{flu}) of the MC540-MnO₂ and MC540-MnO₂-ClO⁻ system, respectively [20].

2.5. The procedure to Determine Anions

Initially, stock solutions were prepared for MnO₂ (1 mg/ml) in pure water and MC540 (1×10^{-3} M) in methanol. Then, a predetermined quantity of MC540's stock solution was transferred into a glass vial, and its solvent was evaporated using argon gas. The MnO₂ solution, at a specific concentration, was then added to this vial. The solution was left undisturbed for 5 minutes to allow for the interaction between MC540 and MnO₂. Absorption and fluorescence spectra were recorded. Thus, a specific MC540-MnO₂ system (2.0×10^{-6} M MC540 and 2.4 μ g/ml MnO₂ in an aqueous solution) was determined for fluorescence sensor studies. Next, various anions (F⁻, Cl⁻, Br⁻, I⁻, S²⁻, NO₃⁻, SO₃²⁻, PO₄³⁻, CO₃²⁻, SCN⁻, CN⁻, AcO⁻, C₂O₄²⁻, and ClO⁻ of 16.7 μ M) were added separately to the specific MC540-MnO₂ system. The prepared solutions were mixed, and fluorescence spectra were immediately recorded for each sample.

2.6. Interference Tests

Interference tests were performed to determine whether other analytes have a positive or negative effect on the response of the major analyte (ClO⁻) to be determined. The fluorescence responses (λ_{flu}) of each MC540-MnO₂-anion (16.7 μ M) system were investigated separately in the presence of ClO⁻ (16.7 μ M).

3. Results and discussion

3.1. Characterization of MnO₂

The formation of MnO₂ was primarily manifested with the disappearance of the purple color of potassium

permanganate and its transformation to dark brown-black color (Fig.2). Then, the resulting MnO₂ was characterized using XRD, FTIR, and absorption spectroscopy. The formation of MnO₂ was first confirmed by the XRD pattern (Fig. 3). The faint peak around $2\theta = 20.63^\circ$ and sharp peaks at $2\theta = 36.55^\circ$, 65.78° , respectively, are reflected (002), (100) and (110) planes of MnO₂ (JCPDS 18-0802) [12, 21-24].

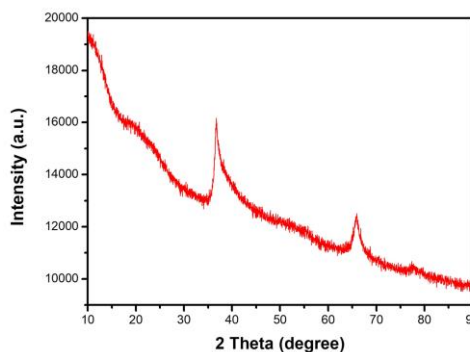


Figure 3. XRD pattern of MnO₂

Secondly, the FTIR spectrum to determine functional groups in the surface of MnO₂ was taken in the wavelength range of 400-4000 cm^{-1} (Fig. 4a). In Fig. 4b, the FTIR peaks are more clearly visible. The wide band at 3380 cm^{-1} is associated with the vibrational existence in hydroxyl groups. The sharp bands at 2926 and 2853 cm^{-1} are due to asymmetric CH₂ stretching vibrations and confirmed that the MnO₂ surface is partially loaded with CTAB. The bands at 1543, 1470, and 1404 cm^{-1} are because of a large amount of hydroxyl groups [25].

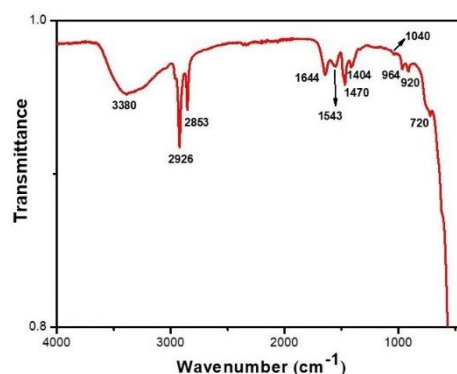


Figure 4. The FT-IR spectra of MnO₂

The band at 1644 cm^{-1} is due to O-H bending vibrations combined with Mn atoms. The bands at 1040, 964, and 920 cm^{-1} demonstrate vibrations due to the interaction of Mn with OH. Furthermore, the intense shoulder bands at 510 and 476 cm^{-1} indicate Mn-O stretching vibrations in the MnO₂ structure [12]. Also, the wide bands at 580 and 720 cm^{-1} are due to the stretching and bending vibrations of the oxide group of MnO₂ in the form of O-Mn-O and Mn-O, respectively [25-27]. Consequently, the data

confirm the formation of MnO_2 NPs and their surface partially loaded with CTAB.

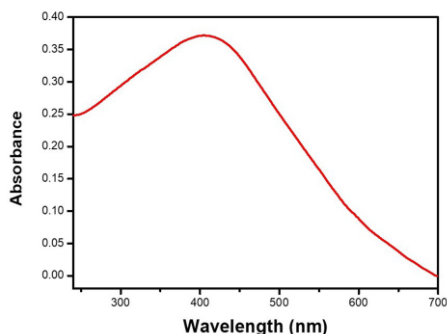


Figure 5. Absorbance spectrum of MnO_2 in aqueous solution (1 mg/ml)

Finally, MnO_2 aqueous solution was characterized by absorption spectroscopy (Fig. 5). The maximum absorption wavelength (λ_{abs}) of MnO_2 , showing absorption in a wide spectrum range of 240 to 700 nm, was determined as ~ 402 nm [14]. This band is the main characteristic band of MnO_2 and could be associated with

the electron transition from the valence band to the conduction band [28, 29]. These characterization data are compatible with MnO_2 structures in the literature.

3.2. Photophysical Properties of MC540 in the presence of MnO_2

The effect of MnO_2 concentration ($[\text{MnO}_2]$) on the molecular behavior of MC540 aqueous dispersion was investigated in the presence of various $[\text{MnO}_2]$ (0.4 – 3.2 $\mu\text{g/mL}$) while MC540 concentration ($[\text{MC540}]$) was kept constant at 2 μM . This effect can be easily understood by comparing it with the MC540's absorption spectrum in pure water.

Here, spectroscopic measurements were performed for 5 min. after mixing $[\text{MnO}_2]$ with MC540. The absorption spectra of MC540 due to the increasing MnO_2 concentration are given in Fig. 6a. As seen in Fig. 6a, two intense absorption band (λ_{abs}) at 535 nm and 503 nm for MC540 in pure water is assigned to monomeric and H-dimeric MC540 molecules.

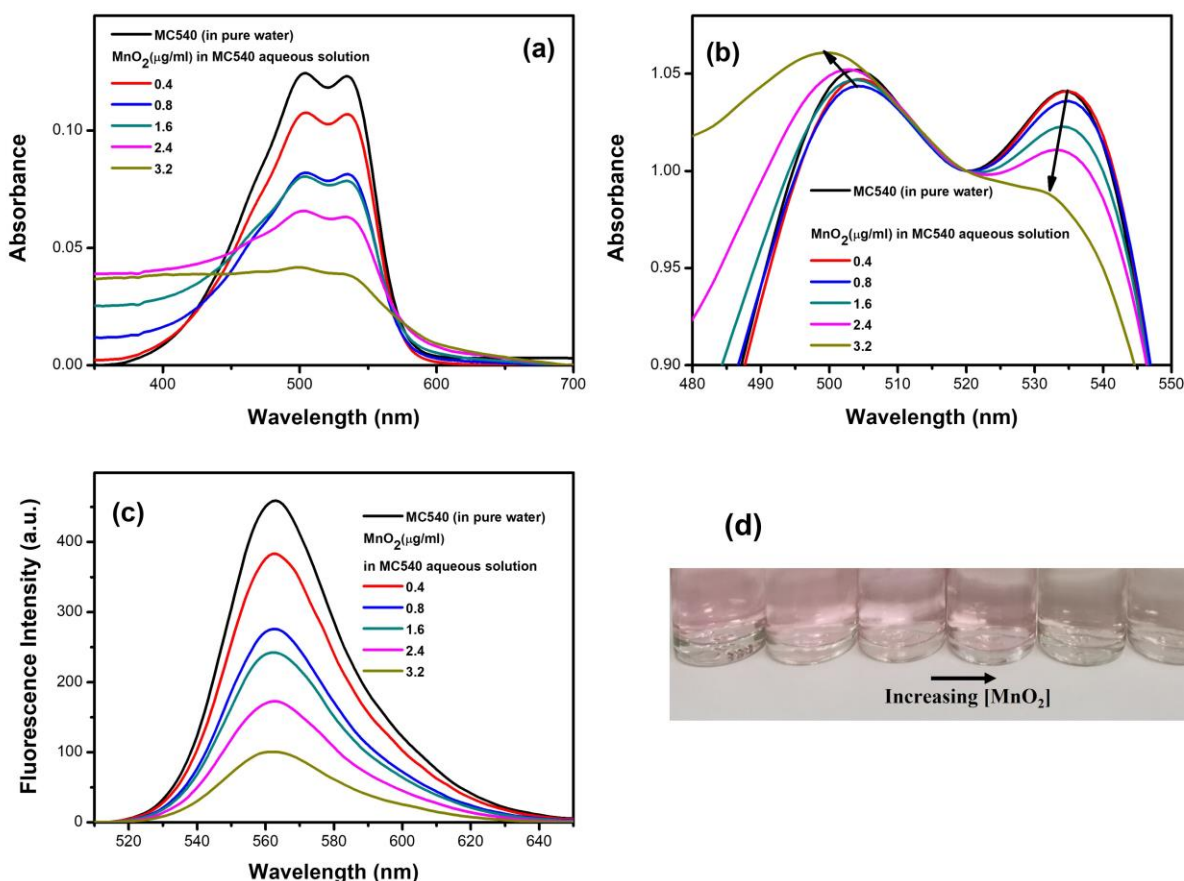


Figure 6. (a) The observed form, (b) the normalized form at 520 nm (isosbestic point) of absorption spectra, (c) fluorescence spectra, and (d) a photograph of MC540 (2 μM) in various $[\text{MnO}_2]$. ($[\text{MnO}_2]$ = 0.04-3.2 $\mu\text{g/mL}$)

When increasing $[\text{MnO}_2]$ is added to the MC540 aqueous solution, it is clearly seen that the MC540 dye molecules

aggregate, its monomer band decreases, and its H-dimer band increases (Fig. 6b). Also, it was determined that the

λ_{abs} of each band were shifted to blue and their intensity decreased significantly. This indicates that $[\text{MnO}_2]$ triggers the dimerization of MC540 by changing its absorption characteristic with strong dipole-dipole interaction in the aqueous medium. Dimers (H-dimer) with low aggregation numbers are commonly referred to as H-aggregates [6]. They are non-fluorescent. For this reason, the effect of $[\text{MnO}_2]$ on the fluorescence properties of MC540 in aqueous dispersion was investigated in the same way as Fig. 6a (Fig. 6c). In Fig. 6c, the effect of $[\text{MnO}_2]$ on the fluorescence of MC540 can be explained by comparing it with the fluorescence spectrum of MC540 aqueous solution. As seen in Fig. 6c, the λ_{flu} of MC540 (2.0×10^{-6} M) in pure water is ~ 562 nm. The λ_{flu} of MC540 is blue-shifted to ~ 1 nm, and the fluorescence intensity of the dye decreased due to the nonradiative transitions by increasing $[\text{MnO}_2]$ in the aqueous dispersions. In addition, the MC540's color change observed with increasing $[\text{MnO}_2]$ is given in Fig. 6d.

Furthermore, the effect of MC540 concentration ($[\text{MC540}]$) was investigated by absorption and fluorescence spectroscopy in various $[\text{MC540}]$ in the range of $1 \mu\text{M}$ - $10 \mu\text{M}$ in the presence of MnO_2 of $2.4 \mu\text{g/mL}$. Absorption spectra of these solutions are given in Fig. 7a. Herein, it is seen that the H-dimer band of the MC540 ($1 \mu\text{M}$) solution containing MnO_2 is at ~ 499 nm,

while its monomer band is at 530 nm. When the $[\text{MC540}]$ was gradually increased, it was determined that its monomeric band red-shifted to 535 nm, while its H-dimer band red-shifted to 503 nm (Fig. 7b). The red shift in the prominent absorption bands of MC540 is due to changes in viscosity, polarity, hydrogen bonding property, and some physical interactions. Moreover, fluorescence spectra of these solutions were taken in the same concentrations (Fig. 7c). In Fig. 7c, when the increase of $[\text{MC540}]$, the λ_{flu} is red-shifted to about 1 nm, and the fluorescence intensity increases. This can be explained by the decrease in $[\text{MnO}_2]$ that could interact with MC540 when the $[\text{MC540}]$ increased. Thus, MC540, which is a monomer-dimer equilibrium, shifted to monomer form with increasing MC540 concentration. The MC540's color change observed with increasing $[\text{MC540}]$ in the presence of MnO_2 ($2.4 \mu\text{g/mL}$) is given in Fig. 7d. In addition, the fluorescence quantum yields of MC540 at increasing MnO_2 and dye concentrations were calculated using their absorption and fluorescence data and are given in Table 1. When Table 1 was examined, with the increase of MnO_2 concentration in MC540 solution, its fluorescence quantum efficiency was seen to be decreased, and thus H-dimerization increased. This is compatible with other data and has proven the interaction of MC540 and MnO_2 in aqueous solution.

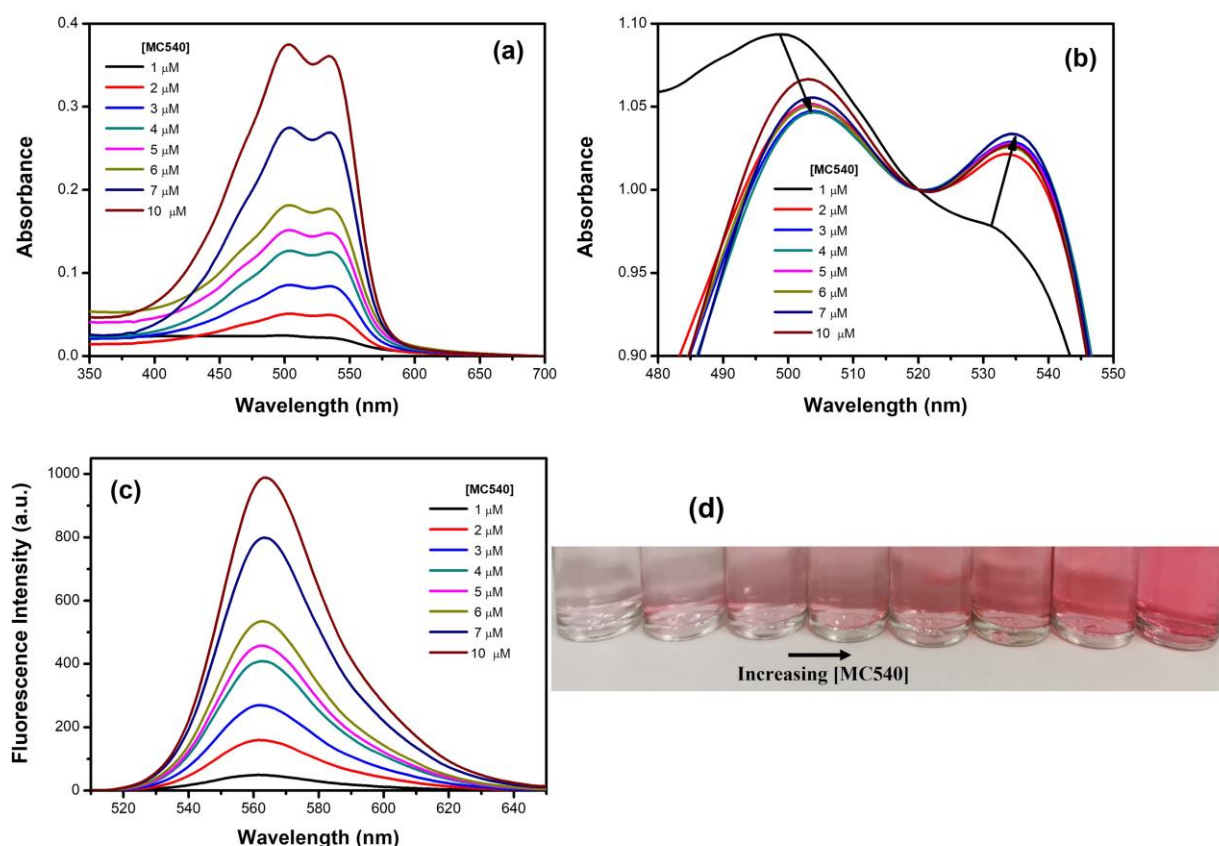


Figure 7. (a) The observed form, (b) the normalized form absorption spectra, (c) the fluorescence spectra, and (d) a photograph of various MC540 solutions containing MnO_2 ($2.4 \mu\text{g/mL}$). ($[\text{MC540}] = 1$ - $10 \mu\text{M}$)

Table 1. Fluorescence quantum yields (Φ_f) of MC540 in aqueous solution in increasing MnO_2 and MC540 concentrations

	Φ_f
[MC540]	
2×10^{-6} M	7.50
[MnO_2]($\mu\text{g/mL}$) ([MC540= 2×10^{-6} M])	
0.4	7.15
0.8	6.51
1.6	5.86
2.4	4.97
3.2	4.43
[MC540](M) ([MnO_2 =2.4 $\mu\text{g/mL}$])	
1×10^{-6}	3.10
2×10^{-6}	4.97
3×10^{-6}	5.20
4×10^{-6}	5.60
5×10^{-6}	5.38
6×10^{-6}	5.41
7×10^{-6}	5.86
10×10^{-6}	5.84

It is decided to use the MC540- MnO_2 system containing [MC540] (2×10^{-6} M) and [MnO_2] (2.4 $\mu\text{g/mL}$), in which MC540 partially dimerized, as a fluorescence probe to detect anions. UV-Vis. absorption and fluorescence spectra for MnO_2 , MC540, and MnO_2 -MC540 systems at the determined concentrations in aqueous solution are comparatively given in Fig. 8a and 8b, respectively.

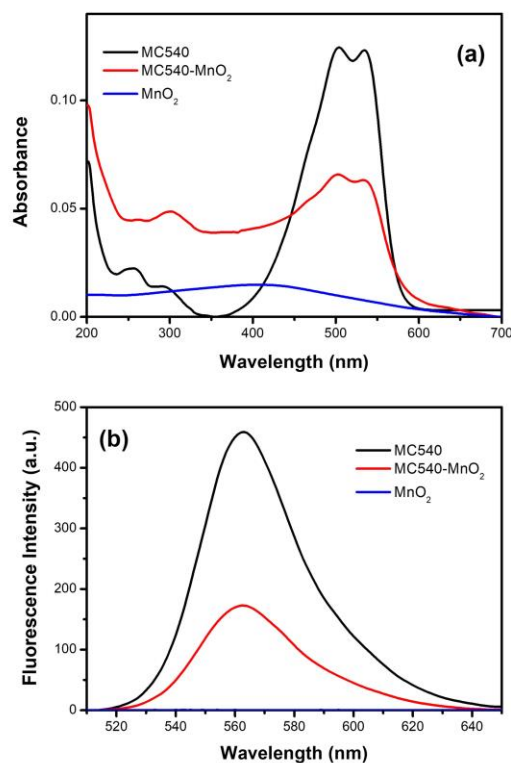


Figure 8. (a) UV-Vis. absorption and (b) fluorescence spectra for MnO_2 , MC540, and MC540- MnO_2 systems

3. 3. Hypochlorite Detection Performance of MC540- MnO_2

The fluorescence spectra of the MC540- MnO_2 aqueous solution were separately taken in the presence of 14 different anions (F^- , Br^- , I^- , Cl^- , SO_4^{2-} , CO_3^{2-} , PO_4^{3-} , NO_3^- , S^{2-} , CN^- , SCN^- , $\text{C}_2\text{O}_4^{2-}$, CH_3COO^- (AcO^-), and ClO^-) to determine of MC540- MnO_2 's selectivity (Fig. 9a). As seen in Fig. 9a, it determined that ClO^- ions quenched the fluorescence intensity of MC540- MnO_2 , whereas other anions had little or no effect. Also, the λ_{flu} was blue-shifted from about ~ 18 nm. This could be due to the formation of a non-radiative complex due to the high affinity of the MC540- MnO_2 fluorescence probe for ClO^- ions. The ClO^- selectivity of MC540- MnO_2 is more clearly shown in the histogram of $(F_0-F)/F_0$ vs. anions, as presented in Fig. 9b. Here, $(F_0-F)/F_0=1$ indicates that the fluorescence intensity of MC540- MnO_2 is completely quenched. When the black columns in Fig. 9b were examined, it was determined that MC540- MnO_2 's fluorescence intensity in the presence of only ClO^- ($\frac{F_0-F}{F_0} \cong 1$) was almost completely quenched. Moreover, interference tests were performed to determine ClO^- , and fluorescence responses of MC540- MnO_2 in the presence of other 13 anions were separately recorded (red columns in Fig. 9b). Thus, ClO^- ions were proven to be detected independently of the other 13 anions.

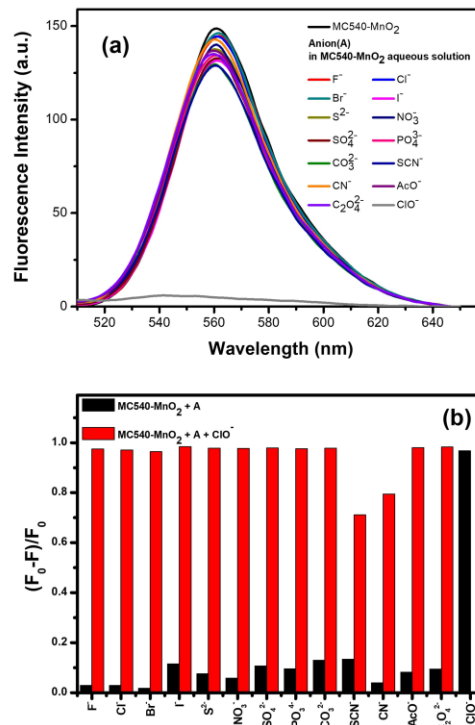


Figure 9. (a) Fluorescence spectra, and (b) histograms of $(F_0-F)/F_0$ vs. anions of MC540- MnO_2 in the absence and presence of various anions, and their ClO^- interference histograms ($\lambda_{\text{ex}} = 500$ nm, $[A]=16.7$ μM , where F_0 and F

are the fluorescence intensities of the MC540-MnO₂ in the absence and presence of anions, respectively).

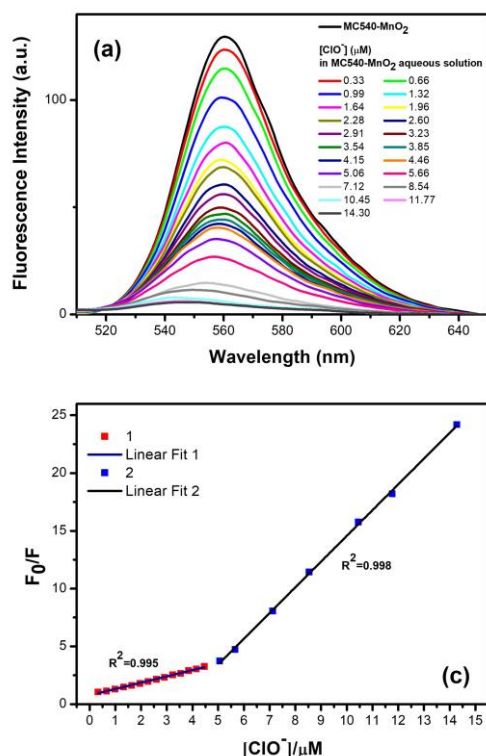


Figure 10. (a) Fluorescence spectra of MC540-MnO₂ system in the presence of various [ClO⁻], and (b) plot of F₀/F vs. [ClO⁻] in the range of 0.33 µM to 14.30 µM.

To test the sensitivity of the MC540-MnO₂ system, the fluorescence spectra of MC540-MnO₂ in ClO⁻ concentration ([ClO⁻]) in the range of 0.33 µM-14.30 µM were recorded (Fig. 10a). In Fig. 10a, it is seen that the fluorescence intensity of MC540-MnO₂ was sensitive to ClO⁻ ions and decreased with increasing [ClO⁻]. In addition, according to Eq. 1, F₀/F vs. [ClO⁻] graph was plotted (Fig. 10b). This graph was non-linear. Therefore, the LOD values were separately determined at two concentration ranges where the F/F₀ vs. [ClO⁻] plot showed high linearity. Each concentration range is indicated in a different color in Fig. 10b, and the correlation coefficients (R²) are given in the graph. The LOD values were calculated as 0.14 µM, and 0.38 µM at [ClO⁻] in the range of 0.33-4.46 µM (1, red) and 5.06-14.30 µM (2, blue), respectively. This indicates that even low concentrations of hypochlorite can be easily detected. Table 2 summarizes the detected ion/molecules, solvent, linear range and LOD values for some fluorescence probes developed for ClO⁻ detection in the literature. In this study, it can be seen that the performance values found for ClO⁻ are better compared to the literature given in Table 2. Consequently, it is determined that the MnO₂-MC540 fluorescence probe in pure water could be a highly accurate and selective "Turn-off" Fluorescence sensor to determine ClO⁻.

Table 2. Various fluorescence probes and their detected ions/molecules in the literature.

Fluorescence probe	Detected ion/molecule	Solvent	Linear range	LOD (µM)	Ref
A coumarin–dihydroperimidine dye	ClO ⁻	Water/MeCN	0-100 µM	3.3 µM	[30]
3-Formyl-10-Methylphenothiazine	ClO ⁻	Water	0-100 µM	0.45 µM	[31]
Red emissive carbon dots	ClO ⁻	Ethanol	0-300 µM	4.95 µM	[32]
N', N'''-((1Z,1'Z)-[2,2'-bithiophene]-5,5'-diylbis(methanylylidene)) bis(furan-2-carbohydrazide)	ClO ⁻	Bis-tris buffer	-	4.2 µM	[33]
Phenothiazine-coumarin platform	ClO ⁻	PBS/ Triton X-100	0-6.5 equiv.	0.321 µM	[34]
MC540-MnO ₂	ClO ⁻	Water	(1) 0.33-4.46 µM (2) 5.06-14.30 µM	(1) 0.14 µM (2) 0.38 µM	This study

4. Conclusions

A new "Turn-off" fluorescence sensor is reported to determine precisely and selectively ClO⁻ based on the interaction of MC540 with MnO₂ in an aqueous solution. Firstly, MnO₂ was synthesized in the presence of KMnO₄ and CTAB using MOPS buffer. The formation of MnO₂ was observed by a color change, and characterized by XRD, FTIR, and absorption spectroscopy. Analysis results showed that it was successfully synthesized. Next, the interaction of MC540 with MnO₂ in various [MnO₂] and [MC540] was studied using UV-Vis. absorption and

fluorescence spectroscopy. The MC540-MnO₂ system containing [MC540] (2x10⁻⁶ M) and [MnO₂](2.4 µg/ml), in which MC540 partially dimerized system, was determined as a fluorescence probe. The sensing ability of the MC540-MnO₂ was separately recorded for their fluorescence responses in the presence of 14 different anions. MC540-MnO₂'s fluorescence intensity was effectively quenched in the presence of only ClO⁻. LOD values for ClO⁻ were evaluated at linear concentration intervals of F₀/F vs. [ClO⁻] plot, and calculated to be 0.14 µM at 0.33-4.46 µM and 0.38 µM at 5.06-14.30 µM, respectively. Interference experiments also showed that

ClO^- could be determined independently of other anions. Thus, it is determined that the MnO_2 -MC540 fluorescence probe in pure water could be a fast and easily applicable, highly accurate, and selective "Turn-off" Fluorescence sensor to determine ClO^- .

Author's Contributions

Ayşe Merve Şenol: Designed the investigation, performed the experiments, and wrote the manuscript.

Ethics

There are no ethical issues after the publication of this manuscript.

References

- [1]. Traven, VF, Cheptsov, DA, and Lodeiro, C. 2023. Control of Fluorescence of Organic Dyes in the Solid-State by Supramolecular Interactions. *J Fluoresc*; 33: 799-847.
- [2]. Korshunov, VM, Mikhailov, MS, Chmovzh, TN, Vashchenko, AA, Gudim, NS, Mikhilchenko, LV, Taydakov, IV, and Rakitin, OA. 2021. Novel D-A-D Fluorescent Dyes Based on 9-(p-Tolyl)-2,3,4,4a,9,9a-hexahydro-1H-carbazole as a Donor Unit for Solution-Processed Organic Light-Emitting-Diodes. *Molecules*; 26: 2872.
- [3]. Tian, Y, Yin, D, and Yan, L. 2023. J-aggregation strategy of organic dyes for near-infrared bioimaging and fluorescent image-guided phototherapy. *Wiley Interdiscip Rev Nanomed Nanobiotechnol*; 15: e1831.
- [4]. Saleem, M, Rafiq, M, Hanif, M, Shaheen, MA, and Seo, S-Y. 2017. A Brief Review on Fluorescent Copper Sensor Based on Conjugated Organic Dyes. *Journal of Fluorescence*; 28: 97-165.
- [5]. Jabeen, U, Shah, SM, Aamir, M, and Ahmad, I. 2021. Grafting and co-grafting of dyes on Cd-doped ZnS nanocrystals and their application on dye-sensitized solar cells. *Bulletin of Materials Science*; 44: 1-9.
- [6]. Bayraktutan, T and Meral, K. 2016. Merocyanine 540 adsorbed on polyethylenimine-functionalized graphene oxide nanocomposites as a turn-on fluorescent sensor for bovine serum albumin. *Phys Chem Chem Phys*; 18: 23400-23406.
- [7]. Su, Y, Mao, Y, Wu, S, Liu, L, and Wen, S. 2023. Silica Coated Upconversion Nanoplatfor for Ag-Based Chemo-/Photodynamic Therapy against Drug-Resistant Bacteria. *ACS Applied Nano Materials*; 6: 8685-8694.
- [8]. Bayraktutan, T, Onganer, Y, and Meral, K. 2016. Polyelectrolyte-induced H-aggregation of Merocyanine 540 and its application in metal ions detection as a colorimetric sensor. *Sensors and Actuators B: Chemical*; 226: 52-61.
- [9]. Wang, H, Liu, Z, Wang, S, Dong, C, Gong, X, Zhao, P, and Chang, J. 2014. MC540 and upconverting nanocrystal coloaded polymeric liposome for near-infrared light-triggered photodynamic therapy and cell fluorescent imaging. *ACS Appl Mater Interfaces*; 6: 3219-25.
- [10]. Valeur, B. 2002. Molecular Fluorescence Principles and Applications; Wiley-Vch Verlag GmbH, Weinheim.
- [11]. Zhang, Y, Zhang, C, Chen, J, Li, Y, Yang, M, Zhou, H, Shahzad, SA, Qi, H, Yu, C, and Jiang, S. 2017. A real-time fluorescence turn-on assay for acetylcholinesterase activity based on the controlled release of a perylene probe from MnO_2 nanosheets. *Journal of Materials Chemistry C*; 5: 4691-4694.
- [12]. Mylarappa, M, Lakshmi, VV, Mahesh, KRV, Nagaswarupa, HP, and Raghavendra, N. 2016. A facile hydrothermal recovery of nano sealed MnO_2 particle from waste batteries: An advanced material for electrochemical and environmental applications. *International Conference on Advances in Materials and Manufacturing Applications (Iconamma-2016)*; 149: 12178.
- [13]. Şenol, AM, Metin, Ö, and Onganer, Y. 2019. A facile route for the preparation of silver nanoparticles-graphene oxide nanocomposites and their interactions with pyronin Y dye molecules. *Dyes and Pigments*; 162: 926-933.
- [14]. Xu, Y, Chen, X, Chai, R, Xing, C, Li, H, and Yin, XB. 2016. A magnetic/fluorometric bimodal sensor based on a carbon dots- MnO_2 platform for glutathione detection. *Nanoscale*; 8: 13414-21.
- [15]. Wang, Y, Jiang, K, Zhu, J, Zhang, L, and Lin, H. 2015. A FRET-based carbon dot- MnO_2 nanosheet architecture for glutathione sensing in human whole blood samples. *Chem Commun (Camb)*; 51: 12748-51.
- [16]. Xiao, T, Sun, J, Zhao, J, Wang, S, Liu, G, and Yang, X. 2018. FRET Effect between Fluorescent Polydopamine Nanoparticles and MnO_2 Nanosheets and Its Application for Sensitive Sensing of Alkaline Phosphatase. *ACS Appl Mater Interfaces*; 10: 6560-6569.
- [17]. Sheng, J, Jiang, X, Wang, L, Yang, M, and Liu, YN. 2018. Biomimetic Mineralization Guided One-Pot Preparation of Gold Clusters Anchored Two-Dimensional MnO_2 Nanosheets for Fluorometric/Magnetic Bimodal Sensing. *Anal Chem*; 90: 2926-2932.
- [18]. Ali, HRH, Hassan, AI, Hassan, YF, and El-Wekil, MM. 2020. One pot fabrication of fluorescein functionalized manganese dioxide for fluorescence "Turn OFF-ON" sensing of hydrogen peroxide in water and cosmetic samples. *RSC Adv*; 10: 17506-17514.
- [19]. Zhou, B, Han, Y, Liu, J, Cheng, K, Dong, M, and Tang, X. 2023. Design and Synthesis of Novel Fluorescent Probe Based on Cyanobiphenyl and its Application in Detection of Hypochlorite. *J Fluoresc*; 33: 575-586.
- [20]. Şenol, AM and Bozkurt, E. 2023. A green "off-on" fluorescent sensor to detect Fe^{3+} and ATP using synthesized carbon dots from Rosehip. *Research on Chemical Intermediates*; 49: 2175-2189.
- [21]. Zhang, X, Miao, W, Li, C, Sun, X, Wang, K, and Ma, Y. 2015. Microwave-assisted rapid synthesis of birnessite-type MnO_2 nanoparticles for high performance supercapacitor applications. *Materials Research Bulletin*; 71: 111-115.
- [22]. Zhou, J, Yu, L, Liu, W, Zhang, X, Mu, W, Du, X, Zhang, Z, and Deng, Y. 2015. High Performance All-solid Supercapacitors Based on the Network of Ultralong Manganese dioxide/Polyaniline Coaxial Nanowires. *Sci Rep*; 5: 17858.
- [23]. Agrawal, R, Adelowo, E, Baboukani, AR, Villegas, MF, Henriques, A, and Wang, C. 2017. Electrostatic Spray Deposition-Based Manganese Oxide Films-From Pseudocapacitive Charge Storage Materials to Three-Dimensional Microelectrode Integrands. *Nanomaterials (Basel)*; 7: 198.
- [24]. Dinh, V-P, Le, N-C, Nguyen, T-P-T, and Nguyen, N-T. 2016. Synthesis of a MnO_2 Nanomaterial from a Precursory- MnO_2 : Characterization and Comparative Adsorption of Pb(II) and Fe(III) . *Journal of Chemistry*; 2016: 1-9.
- [25]. Mahmoud, ME, Khalifa, MA, El-Mallah, NM, Hassouba, HM, and Nabil, GM. 2021. Performance of MnO_2 nanoparticles-

- coated cationic CTAB for detoxification and decolorization of sulfonated remazol red and reactive black 5 dyes from water. *International Journal of Environmental Science and Technology*; 19: 141-158.
- [26]. Said, MI, Rageh, AH, and Abdel-Aal, FAM. 2018. Fabrication of novel electrochemical sensors based on modification with different polymorphs of MnO(2) nanoparticles. Application to furosemide analysis in pharmaceutical and urine samples. *RSC Adv*; 8: 18698-18713.
- [27]. Xie, Y, Yu, Y, Gong, X, Guo, Y, Guo, Y, Wang, Y, and Lu, G. 2015. Effect of the crystal plane figure on the catalytic performance of MnO₂ for the total oxidation of propane. *CrystEngComm*; 17: 3005-3014.
- [28]. Sorouri, F, Gholibegloo, E, Mortezaazadeh, T, Kiani, S, Foroumadi, A, Firoozpour, L, and Khoobi, M. 2023. Tannic acid-mediated synthesis of flower-like mesoporous MnO(2) nanostructures as T(1)-T(2) dual-modal MRI contrast agents and dual-enzyme mimetic agents. *Sci Rep*; 13: 14606.
- [29]. Godlaveeti, SK, Komatikunta, VK, Somala, AR, Sangaraju, S, Alshgari, RA, Mushab, MSS, Maseed, H, and Nagireddy, RR. 2023. Different Phase and Morphology of the MnO₂ on Various Substrates and Electrolytes for Electrochemical Performance. *Journal of Cluster Science*; 34: 2725-2736.
- [30]. Shiraishi, Y, Yamada, C, and Hirai, T. 2019. A coumarin-dihydroperimidine dye as a fluorescent chemosensor for hypochlorite in 99% water. *RSC Adv*; 9: 28636-28641.
- [31]. Song, H, Zhou, Y, Xu, C, Wang, X, Zhang, J, Wang, Y, Liu, X, Guo, M, and Peng, X. 2019. A dual-function fluorescent probe: Sensitive detection of water content in commercial products and rapid detection of hypochlorite with a large Stokes shift. *Dyes and Pigments*; 162: 160-167.
- [32]. Zhu, Y, Li, G, Li, W, Luo, X, Hu, Z, and Wu, F. 2023. Facile synthesis of efficient red-emissive carbon quantum dots as a multifunctional platform for biosensing and bioimaging. *Dyes and Pigments*; 215: 111303.
- [33]. Kim, PA, Choe, D, So, H, Park, S, Suh, B, Jeong, S, Kim, KT, Kim, C, and Harrison, RG. 2021. A selective fluorescence sensor for hypochlorite used for the detection of hypochlorite in zebrafish. *Spectrochim Acta A Mol Biomol Spectrosc*; 261: 120059.
- [34]. Wang, W, Ning, J-Y, Liu, J-T, Miao, J-Y, and Zhao, B-X. 2019. A mitochondria-targeted ratiometric fluorescence sensor for the detection of hypochlorite in living cells. *Dyes and Pigments*; 171: 107708.